JOURNAL OF AIRCRAFT
Vol. 30, No. 5, Sept.–Oct. 1993

Multielement Airfoil Performance Due to Reynolds and Mach Number Variations

Walter O. Valarezo* and Chet J. Dominik†
Douglas Aircraft Company, Long Beach, California 90846
and
Robert J. McGhee‡
NASA Langley Research Center, Hampton, Virginia 23665

Experimental studies have been conducted to assess Reynolds and Mach number effects on a supercritical multielement airfoil. The airfoil is representative of the stall-critical station of an advanced transport wing design. The experimental work was conducted as part of a cooperative program between the Douglas Aircraft Company and the NASA Langley Research Center to improve current knowledge of high-lift flows and to develop a validation data base with practical geometries/conditions for emerging computational methods. This article describes results obtained for both landing and takeoff multielement airfoils (four- and three-element configurations) for a variety of Mach/Reynolds number combinations up to flight conditions. Effects on maximum lift are considered for the landing configurations, and effects on both lift and drag are reported for the takeoff geometry. The present test results revealed considerable maximum lift effects on the three-element landing configuration for Reynolds number variations, and significant Mach number effects on the four-element airfoil.

Nomenclature

C_d = drag coefficient
C_l = lift coefficient
$C_{l\max}$ = maximum lift coefficient
C_p = pressure coefficient
C_P^* = critical pressure coefficient
L/D = lift-to-drag ratio
M = Mach number
RN = chord Reynolds number
α = angle of attack
δ_f = flap deflection
δ_s = slat deflection

Introduction

COMMERCIAL transport aircraft wings are configured with leading-edge slats and trailing-edge flaps to meet takeoff and landing operational requirements. High-lift systems have traditionally been complex in order to attain the aerodynamic capability of generating high L/D in climb, and high maximum lift on approach. However, increased financial pressures in the airline business demand high-lift wing designs that are simpler and easier to maintain, while achieving improved aerodynamic performance over previous-generation designs. A major obstacle in the design process towards more efficient multielement airfoils has been the lack of published data on the effects of Reynolds and Mach number over a realistic range for representative multielement airfoils. This lack of data is also likely to have delayed the development of computational methods suitable for the analysis of practical multielement airfoils at conditions of interest (maximum lift). Several purely computational methods have been recently reported in the literature[1–10] that can handle, to various degrees of success, the viscous flow over multielement airfoils. However, these methods have largely been applied to either geometries that are not really representative of transport high-lift airfoils or to flow conditions that do not include maximum lift. It is expected that some of these methods (either Navier-Stokes or boundary-layer based) hold significant promise, but may not be substantially improved by their developers in the absence of a quality data base at realistic conditions for a practical airfoil. The work reported in this article is the result of a cooperative experimental program conducted by the Douglas Aircraft Company and the NASA Langley Research Center to establish a data base for Reynolds and Mach number (including flight condition) effects on the flow over transport multielement airfoils.

Test Facility and Model Description

The Langley low turbulence pressure tunnel (LTPT) is a single-return, closed-throat wind tunnel that can be operated up to 10 atmospheres, thus allowing very high Reynolds number capability[11] (Fig. 1). The test section is 3-ft wide by 7.5-ft high by 7.5-ft long. To promote two-dimensional flow over the model in view of its low-aspect ratio and strong wall-model aerodynamic interference, a new side-wall boundary-layer control (BLC) system was installed at the LTPT for the present test.[12] The BLC system employed the differential pressure between the test section and the atmosphere to provide suction of the boundary layer through porous endplates. The system yielded good quality two-dimensional flow over the model for the Reynolds numbers tested.[12] The model spanned the width of the test section and had a clean (stowed) airfoil chord of 22 in. The clean airfoil and the takeoff and landing multielement configurations tested are shown in Fig. 2. The slat chord ratio was 14.48%, the single-segment flap chord ratio was 30%, and the two-segment flap had a chord ratio of 21% for the main segment and 13% for the auxiliary flap. Pressure orifices were located along the centerline of the model (142 taps for the four-element configuration). Additionally, pressure taps were located along (or near) the trailing edge of each airfoil element to monitor two-dimensionality of the flow at run time. Integration of the pressure measurements yielded the forces presented here.

The data is corrected for the effects of the sidewall suction system on the tunnel parameters. The LTPT wake survey apparatus is a recent addition to the tunnel and had only been

Received Feb. 20, 1992; revision received May 31, 1992; accepted for publication July 2, 1992.

*Principal Technical Specialist, Team Leader-Subsonics and High Lift, Aerodynamics Technology. Senior Member AIAA.
†Engineer/Scientist, Aerodynamics Technology. Member AIAA.
‡Section Head, Low-Turbulence Pressure Tunnel, Experimental Flow Physics Branch.

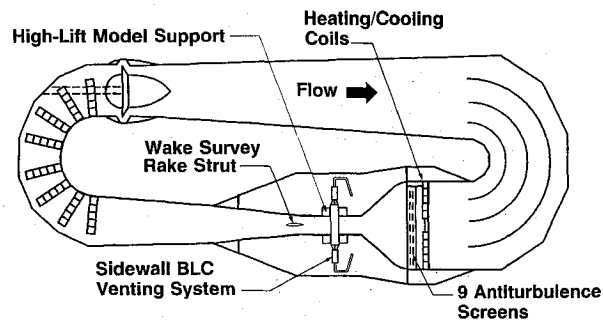

Fig. 1 Schematic of low turbulence pressure tunnel.

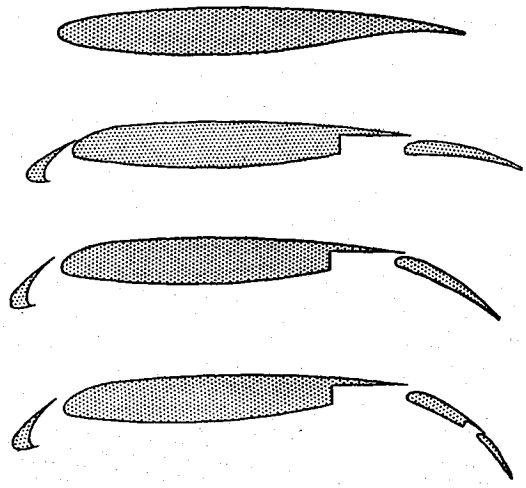

Fig. 2 Airfoil configurations tested in the LTPT.

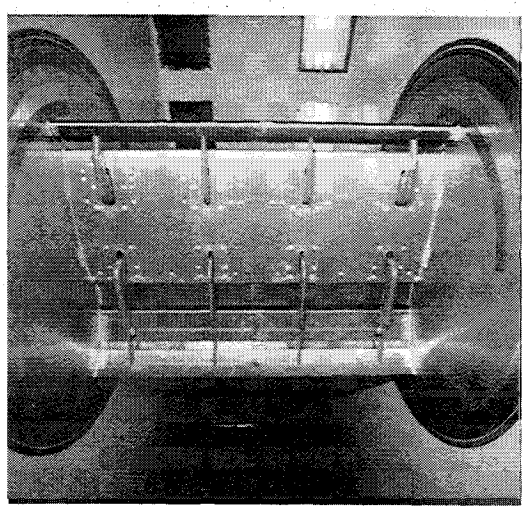

Fig. 3 LTPT high-lift model support brackets.

partially checked out at the time of this test, therefore, no wake survey data were available for some configurations tested. Due to the partial lack of drag data, no wake blockage correction could be derived for some of the cases. Therefore, to be consistent, the data shown here does not include wake blockage corrections. This is not expected to change the performance trends shown in this article. However, specific cases selected for detailed computational fluid dynamics (CFD) validation would require such corrections.

Four rows of streamlined support brackets for the high-lift devices (Fig. 3) were required due to the very high loads (up to 15,000 lb) associated with the high freestream dynamic pressure and lift coefficients attained. In expectation of these loads, the four sets of brackets were sized and spaced such that component aeroelastic deflections would be minimal. Additionally, leading- and trailing-edge components were fabricated from 17-4PH stainless steel. Drag data were computed by integration of the static and total pressures obtained from the LTPT wake survey rake system.[13]

Data repeatability at the LTPT is ± 0.02 in maximum lift coefficient and ± 0.0010 in drag coefficient for landing configurations.

Results

A significant percentage of the wind-tunnel testing associated with multielement airfoils is aimed at optimizing the rigging of a particular airfoil with fixed slat and flap chord ratios. Parameters defining rigging nomenclature for multielement airfoils are shown in Fig. 4. The gap is the minimum distance between the trailing edge of a forward element and any point on the surface of the trailing element. The overhang can be positive (overlap) or negative (no overlap), and together with the gap is expressed as a fraction of stowed airfoil chord. The optimization work is traditionally performed at a given Mach/Reynolds number that should be representative of nominal flight conditions. However, it is also very important to determine the effects on the performance of the optimized airfoil for departures in Reynolds or Mach number from the nominal conditions. It was possible to perform these measurements (Reynolds and Mach number sweeps) at the LTPT because of its considerable operational capability (Fig. 5).

Transition strips were not utilized due to the ability of the LTPT to provide flight Reynolds numbers. All results shown here were obtained transition-free.

The effects of Reynolds number on the clean airfoil maximum lift capability at various Mach numbers is shown in Fig. 6. It can be seen that there is a considerable increase in maximum lift between Reynolds numbers of 2.5×10^6 and 9×10^6. Corresponding surface pressures on the clean airfoil at maximum lift are shown in Figs. 7 and 8. For the 0.20 freestream Mach number, C_P^* is -16.3, and for the 0.32 Mach condition C_P^* is -6.03. Compressibility does not appear to

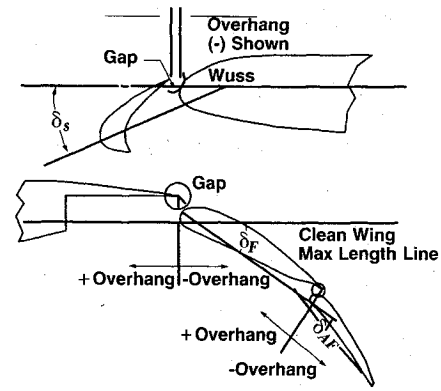

Fig. 4 Nomenclature for multielements.

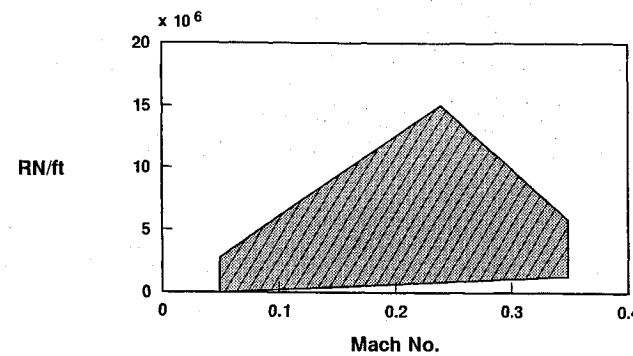

Fig. 5 Operational capability of the LTPT.

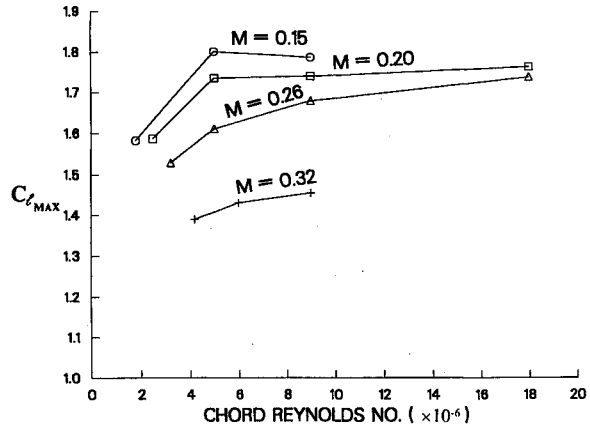

Fig. 6 Reynolds number effect on maximum lift.

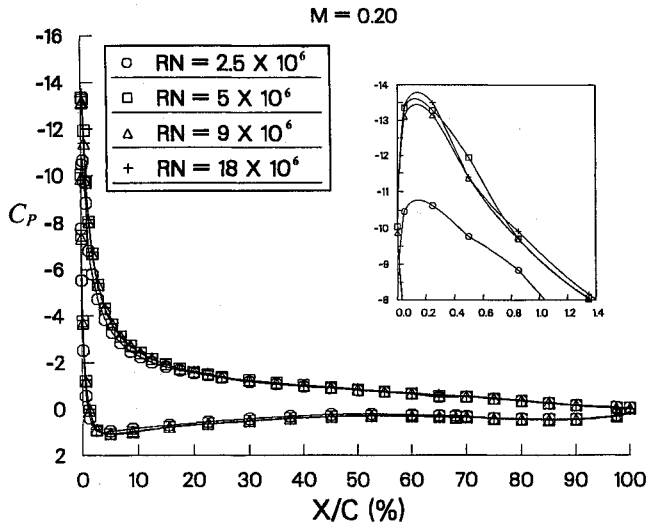

Fig. 7 Reynolds number effect at maximum lift.

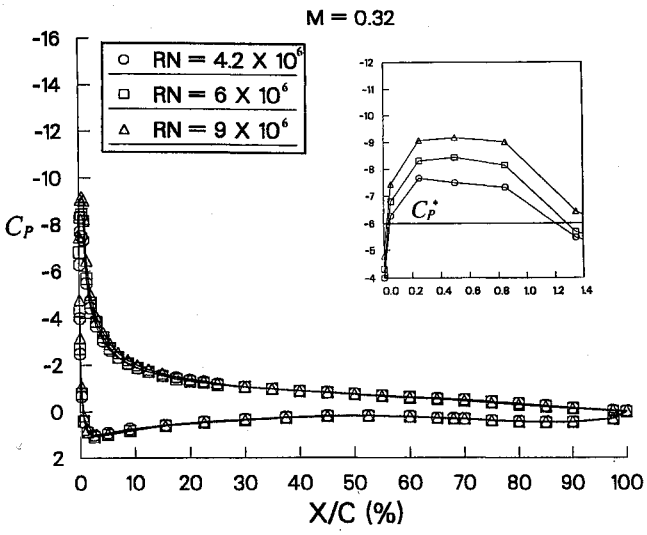

Fig. 8 Reynolds number effect at maximum lift.

have a major influence on maximum lift at a freestream Mach number of 0.20 or below. The effects of Mach number on maximum lift are shown in Fig. 9 for Reynolds numbers from 5 to 18 × 10^6. It can be seen that the effect of Mach number is substantially more pronounced at the lower Reynolds numbers.

These results shown for the basic clean airfoil (Figs. 6–9) served to establish a baseline for both Reynolds and Mach

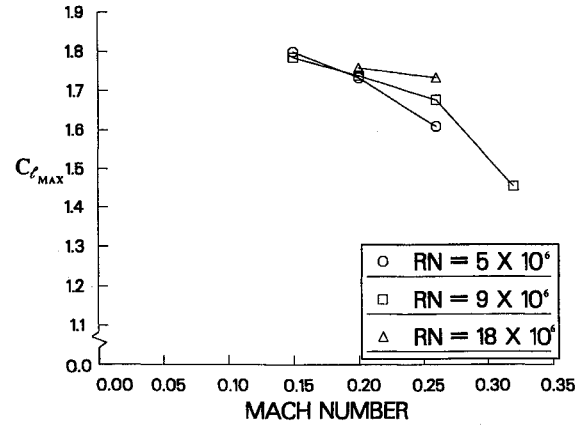

Fig. 9 Mach number effect on maximum lift.

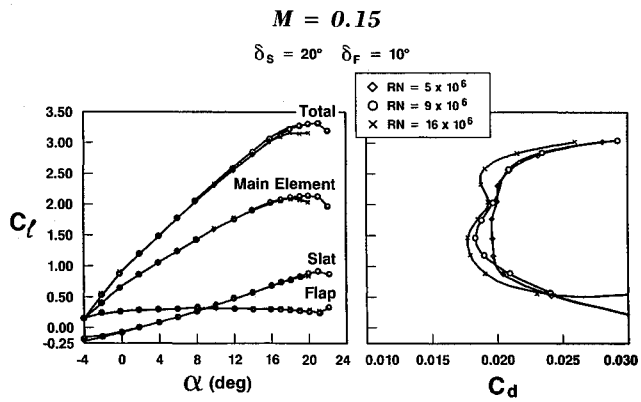

Fig. 10 Reynolds number effect.

number effects for the subsequent multielement airfoil measurements and they may also represent a logical starting point for the validation of any viscous flow method, since surface grid complications are at a practical minimum and flow features through the maximum lift condition are still complex enough to be of interest.

Takeoff Configuration

A three-element airfoil configured for takeoff was tested at various combinations of Reynolds and Mach number as shown below:

	Freestream Mach Number				
RN × 10^{-6}	0.15	0.20	0.26	0.30	0.32
5	x	x	x	x	
9	x	x	x	x	x
16	x	x			
20		x			

The slat deflection was 20 deg (gap = 0.55%, overhang = +1.0%), and the flap was rigged at a gap of 1.82%, overhang of 1.5%, and 10 deg of deflection. For a takeoff configuration the slat is normaly sealed (gap = 0%) to minimize profile drag, however, an open slat was chosen for this study since it should be less difficult to grid from a computational analysis perspective. Additionally, this particular open slat configuration yielded takeoff performance close to that of a sealed slat at a representative lift coefficient.

Lift curves and drag polars for Reynolds numbers from 5 to 16 × 10^6 at Mach 0.15 are shown in Fig. 10. There is a loss in maximum lift and improved drag performance with increasing Reynolds number. It is also interesting to note that while the main element enters the stall first, it is soon followed by the slat and not the flap. In fact, the flap lift coefficient

increases after the stall. This effect appears to be due to the drastically reduced downwash from both the slat and the main element, and the fact that the geometric deflection of the flap (10 deg) is not enough by itself to cause the flow on the flap to separate.

Reynolds number effects on lift and drag obtained at Mach 0.20 are shown in Fig. 11. Here, it is evident that the Reynolds number effect is largely on drag and not on lift. Differences in measured drag are approximately 10% between the 5×10^6 and the 20×10^6 Reynolds numbers. Again, the flap loads up after the main element and the slat enter the stall. In fact, it is now clear that the flap loads up after the slat stalls. Results at Mach 0.26 and 0.30 are shown in Figs. 12 and 13, respectively. At these two Mach numbers, the Reynolds number effect is to increase maximum lift (opposite trend from Mach 0.15) but, in general, the Reynolds number effect on either lift or drag is minimal. It is worth noting that at these conditions, even though the main element exhibits a pronounced stall, the slat does not, and the flap displays only a slight tendency to load up beyond the stall. That the slat does not

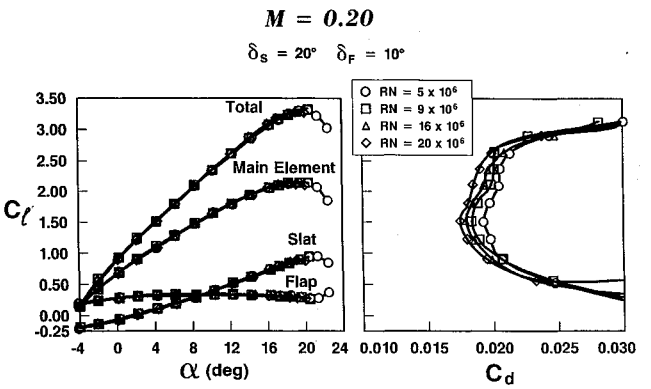

Fig. 11 Reynolds number effect.

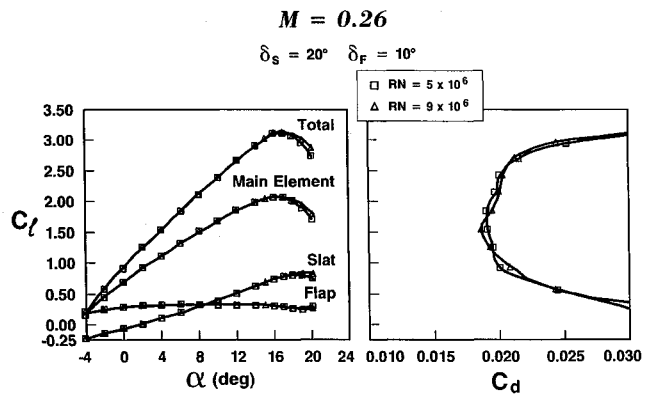

Fig. 12 Reynolds number effect.

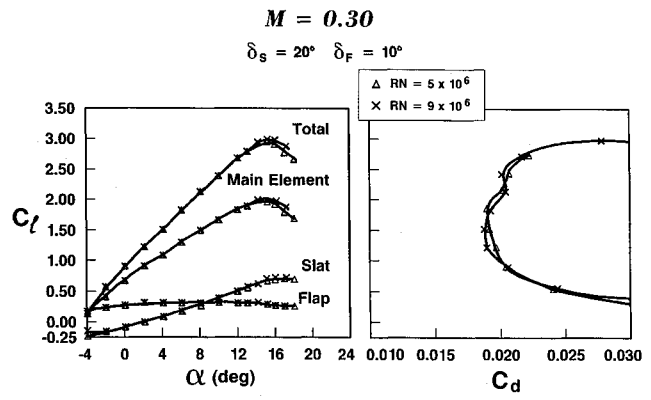

Fig. 13 Reynolds number effect.

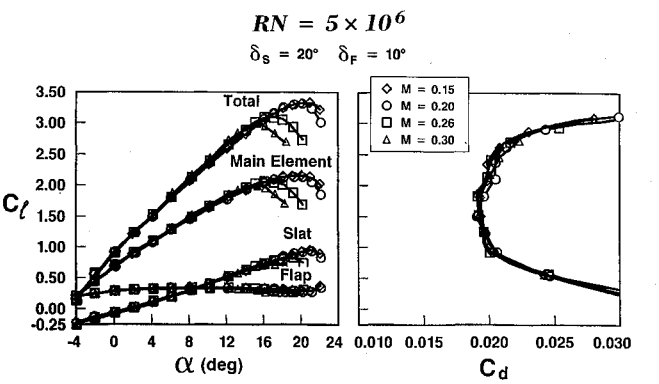

Fig. 14 Mach number effect.

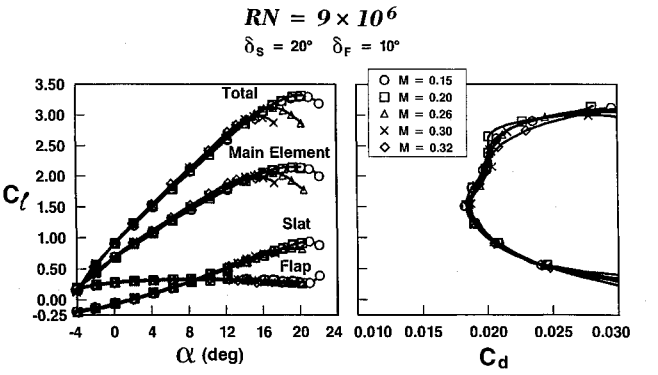

Fig. 15 Mach number effect.

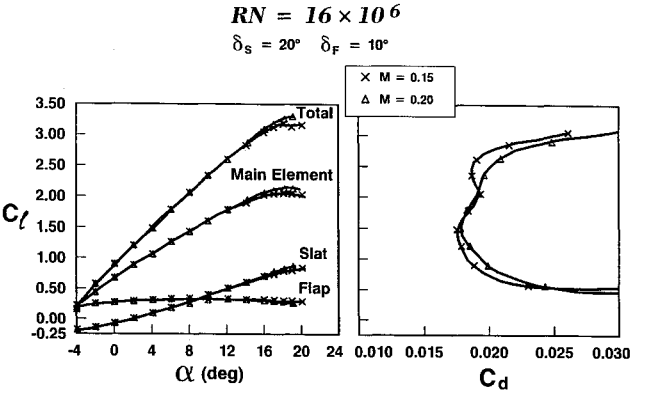

Fig. 16 Mach number effect.

really stall, as it did at lower Mach numbers, is a result of the slat being exposed to a lower geometric angle of attack (lower airfoil stall angles at higher Mach numbers). Mach number effects on the takeoff configuration at Reynolds numbers of 5×10^6, 9×10^6, and 16×10^6 are shown in Figs. 14, 15, and 16, respectively. Overall, the measured effect of Mach number on C_d at a given Reynolds number can be seen to be in the scatter band of the data (within 10 counts). However, the Mach effect on lift is substantial.

Landing Configurations

Two landing configurations were selected for Reynolds and Mach number effects studies. The leading-edge slat was optimized for both configurations, and was positioned at a gap of 2.95% with an overhang of −2.5% and 30 deg of deflection.

The single-segment flap airfoil was configured with the flap optimized at a Reynolds number of 9×10^6 at 30 deg of deflection with a gap of 1.32% and an overhang of +1.0%. A Reynolds number sweep was conducted at Mach 0.20, and effects on maximum lift are shown in Fig. 17. There is a considerable loss in $C_{l\max}$(~0.1) at Reynolds numbers other

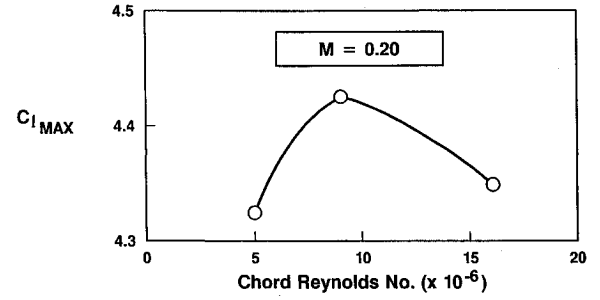

Fig. 17 Reynolds number effect on configuration optimized at RN = 9 × 10^6 (δ_s = 30 deg, δ_f = 30 deg).

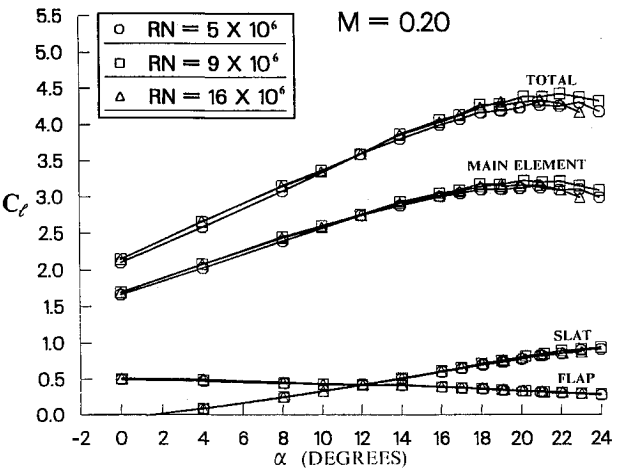

Fig. 18 Reynolds number effect on lift (δ_s = 30 deg, δ_f = 30 deg).

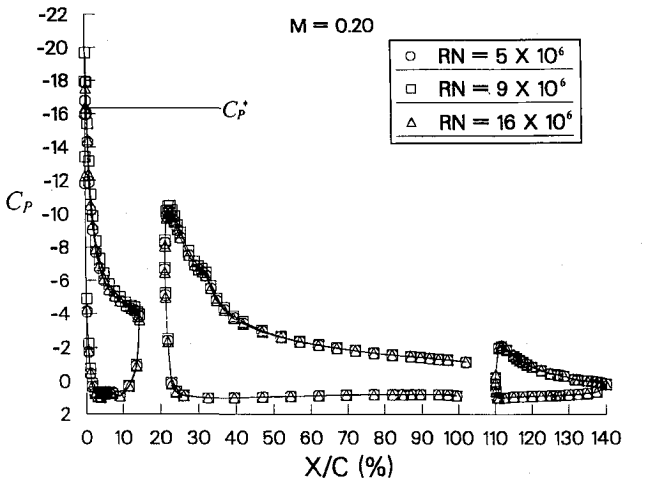

Fig. 19 Reynolds number effect on lift (δ_s = 30 deg, δ_f = 30 deg).

than 9 × 10^6. Total and component loadings are shown in Fig. 18 where it can be seen again that the airfoil stall is caused by the main element. Unlike the takeoff cases reviewed above, the slat continues to load up beyond the airfoil stall. This is possibly due to the slat position being aerodynamically underdeflected (−10 deg) with respect to the takeoff slat discussed. Surface pressure measurements obtained at the three Reynolds numbers at maximum lift are shown in Fig. 19. Although the data are closely matched, being able to discern a difference of 0.10 in $C_{l_{max}}$ performance is of considerable importance in transport high-lift aerodynamics.

The second landing arrangement tested was a four-element airfoil with a two-segment flap. The optimum slat position was the same as for the three-element landing airfoil. The main flap was optimized at 35 deg with a gap of 2.9% and an

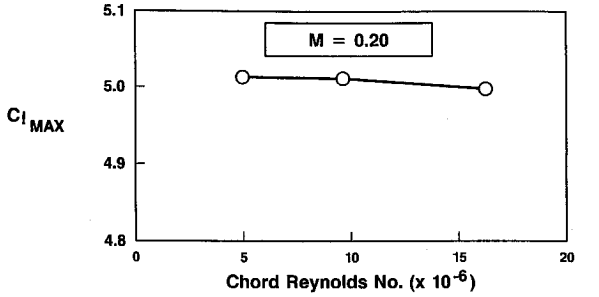

Fig. 20 Reynolds number effect on maximum lift (δ_s = 30 deg, δ_f = 35 deg/15 deg).

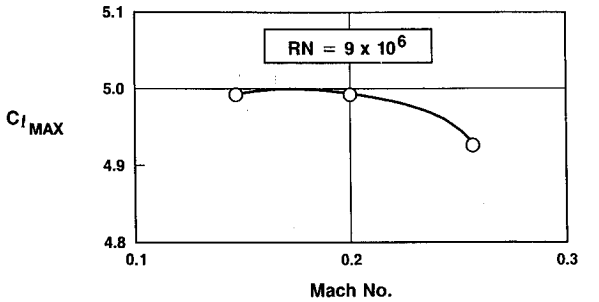

Fig. 21 Mach number effect on maximum lift (δ_s = 30 deg, δ_f = 35 deg/15 deg).

overhang of −1%. The auxiliary flap was deflected an additional 15 deg and had a nonoptimized gap of 0.68% and an overhang of 0.75%. Reynolds number effects at 0.20 Mach number are shown in Fig. 20. It is evident that the effects of Reynolds number on maximum lift are minimal for the Reynolds number range tested. This can be contrasted with the substantial Reynolds number effects shown for the single-segment flap configuration. It is possible that this difference in dependence on Reynolds number could be due to the large optimum gap for the two-segment flap and the much smaller (approximately half) optimum gap for a single-segment flap. These different gaps represent different enough slot geometries between the main element and the flap which could lead one configuration (single-segment flap) to be more Reynolds number sensitive than the other.

The effect of Mach number on maximum lift at a Reynolds number of 9 × 10^6 is shown in Fig. 21. It was observed that increasing Mach number caused reductions in both maximum lift and stall angle.

Experimental studies of the effects of Reynolds and Mach number variations on the performance of a practical transport-type multielement high-lift airfoil have been presented. The studies were conducted at the NASA Langley Low Turbulence Pressure Tunnel under a cooperative program between the Douglas Aircraft Company and the NASA Langley Research Center to establish a high-quality data base for these effects that can be used in the calibration/validation of computational methods in development for practical multielemental airfoil configurations. Salient findings of the present work are as follows:

1) Reynolds number effects are significant even on the single-element airfoil below 5 × 10^6 Reynolds number.

2) Mach number effects were more pronounced at the lower Reynolds numbers.

3) Extensive Reynolds and Mach number surveys were conducted on a three-element takeoff configuration (δ_s = 20 deg, δ_f = 10 deg). In general, Reynolds number effects on both lift and drag were minimal, but different trends were exhibited depending on the Mach number. Mach number effects on maximum lift were substantial.

4) For the three-element takeoff configuration, the main element of the airfoil enters the stall first and is followed by the slat stalling. The flap does not stall.

5) Significant Reynolds number effects were apparent for the three-element landing configurations. As observed in the takeoff work, the main element of the airfoil stalls first. However, both the slat and flap continue to load up after the main element stalls.

6) Mach number effects on the four-element landing configuration were substantial. Reynolds number effects were not as large as those measured on the three-element airfoil.

References

[1]Cebeci, T., Chang, K. C., Clark, R. W., and Halsey, N. D., "Calculation of Flow over Multielement Airfoils at High Lift," International Council of Aeronautical Sciences, Paper 86-2.3.1.

[2]Shima, E., "Numerical Analysis of Multiple Element High Lift Devices by Navier Stokes Equation Using Implicit TVD Finite Volume Method," AIAA Paper 88-2574-CP, June 1988.

[3]Wang, G., Wu, J., and Tung, C., "A Numerical Study of General Viscous Flows Around Multi-Element Airfoils," AIAA Paper 90-0572, Jan. 1990.

[4]Drela, M., "Newton Solution of Coupled Viscous/Inviscid Multielement Airfoil Flows," AIAA Paper 90-1470, June 1990.

[5]Mavriplis, D. J., "Algebraic Turbulence Modeling for Unstructured and Adaptive Meshes," AIAA Paper 90-1653, June 1990.

[6]Mavriplis, D. J., "Turbulent Flow Calculations Using Unstructured and Adaptive Meshes," NASA CR 182102, Sept. 1990.

[7]Mavriplis, D. J., "Multigrid Solution of Compressible Turbulent Flow on Unstructured Meshes Using a Two-Equation Model," AIAA Paper 91-0237, Jan. 1991.

[8]Kusunose, K., Wigton, L., and Meredith, P., "A Rapidly Converging Viscous/Inviscid Coupling Code for Multi-Element Airfoil Configurations," AIAA Paper 91-0177, Jan. 1991.

[9]Chow, R., and Chu, K., "Navier-Stokes Solution for High-Lift Multielement Airfoil System with Flap Separation," AIAA Paper 91-1623, June 1991.

[10]Cebeci, T., Jau, J., and Vitiello, D., "An Interactive Boundary-Layer Approach to Multielement Airfoils at High Lift," AIAA Paper 92-0404, Jan. 1992.

[11]Valarezo, W. O., Dominik, C. J., McGhee, R. J., Goodman, W. L., and Paschal, K. B., "Multielement Airfoil Optimization for Maximum Lift at High Reynolds Numbers," AIAA Paper 91-3332, Sept. 1991.

[12]Paschal, K. B., Goodman, W. L., McGhee, R. J., Walker, B., and Wilcox, P. A., "Evaluation of Tunnel Sidewall Boundary-Layer Control Systems for High-Lift Airfoil Testing," AIAA Paper 91-3243, Sept. 1991.

[13]Friedman, I. P., "Calibration and Application of a New Wake Rake System for Drag Measurement of High Lift Airfoil Models," M.S. Thesis, School of Applied Engineering and Applied Sciences, George Washington Univ., Washington, DC, April 1991.